Eur. Phys. J. D **26**, 59–65 (2003)
DOI: 10.1140/epjd/e2003-00249-7

THE EUROPEAN PHYSICAL JOURNAL D

Statistical investigations of the beam stability of the double-pass amplified zinc soft X-ray laser at 21.2 nm

A.R. Präg[a], T. Mocek, M. Kozlová, B. Rus, and K. Rohlena

PALS, Institute of Physics, Academy of Sciences, Na Slovance 2, 18221 Prague 8, Czech Republic

Received 20 November 2002 / Received in final form 16 April 2003
Published online 5 August 2003 –

Abstract. At the Prague asterix laser system (PALS) of the Academy of Sciences of the Czech Republic the 1-TW asterix iodine laser is used as a pump source for soft X-ray laser experiments. The prepulse technique was applied which is known to enhance the X-ray laser output at the $J = 0$–1 transition dramatically. Since Zn slab targets were used the laser wavelength was 21.2 nm. A prepulse beam having 1.6 J was preceding the main pulse by 10 ns. The main and the prepulse beam are focused by two different optical systems separately. Implementing a half-cavity set-up for double-pass amplification using a Mo/Si multilayer mirror the X-ray laser output was 10 times stronger than at single pass amplification in a 3-cm long plasma. Double-pass amplification was observed to be most efficient when the pump pulse duration was at least 120 ps longer than the round trip time in the half-cavity. Under this fundamental condition the X-ray laser reached saturation in the double-pass regime containing 4 mJ energy what is proved to be enough for applications. In this contribution the X-ray laser features like divergence in two dimensions, the beam quality (symmetry), the pointing angle and the time-integrated output energy are investigated over more than 100 shots. To characterize the stability of the X-ray laser the shot distribution, the mean value and the standard deviation for these parameters are evaluated. For 18 shots in a series — achieved during one single day — the corresponding values are given and detailed chi-squared tests characterize the Zn X-ray laser as a robust tool suitable for applications. At PALS soft X-ray laser beam time can be reserved for external research groups.

PACS. 42.55.Vc X- and γ-ray lasers – 42.60.Da Resonators, cavities, amplifiers, arrays, and rings – 42.60.Jf Beam characteristics: profile, intensity, and power; spatial pattern formation

1 Introduction

In a couple of laboratories several types of X-ray lasers (XRL) were developed [1]. Using collisional excitation XRL over a broad wavelength range were realised in Ne-like [2–6] and Ni-like ions [7,8]. Applying traveling wave geometry the pumping method was modified to the transient collisional excitation (TCE) [9–12]. Another type is based on capillary-discharges where lasing takes place in a gas-filled capillary driven by a high-current pulse. Table-top lasing at 46.9 nm in Ne-like Ar was attained with this method [13,14]. Another method is realised by using ultrashort pulses to induce optical-field ionisation in Pd-like Xe [15]. In this work we use the prepulse technique which improves the XRL output considerably [2]. We examine the double-pass amplified Ne-like Zn at 21.2 nm, using 3-cm long laser-plasma and a half-cavity set-up which is suitable to saturate the Zn XRL output [5].

The diversified application of XRL is coupled to the condition of an appropriate stability of beam parameters (beam size, divergence, symmetry, pointing angle, energy, coherence and pulse duration) being reproducible from shot to shot. When long-pulse systems at low rep-rate are used mainly single-shot results are published. However, a considerable shot-to-shot fluctuation was reported [16], but without analysing the reasons in detail. Despite possible reasons for the fluctuations (pump laser instabilities, scattering of pulse duration, degradation of optical components due to damage) in this contribution we study the stability over 110 shots, at a low rep-rate of 20 minutes between two shots. Nevertheless, the low rep-rate constitutes a considerable disadvantage for the statistical analysis, because the confidence into statistics is increasing with the size of the random sample gained in a rational time. Typical values for the XRL beam divergences reported recently are between 2.2 and 3.6 mrad for Ni-like Ag in horizontal direction and between 5 and 6 mrad in vertical direction [8]. Generally for the vertical divergence a higher value was measured than for the horizontal divergence [1,14]. Defining a dimensionless parameter, *i.e.* the *beam symmetry* as the ratio of horizontal to vertical

[a] e-mail: praeg@fzu.cz

divergence, a value clearly < 1 was obtained. This result is due to the asymmetric plasma expansion in either direction (parallel or perpendicular to the target surface). Due to the same context from two-dimensional near-field images can be extracted that the gain region in the plasma is in the direction parallel to the target larger than perpendicularly [10]. Double-pass amplification applying a two-target geometry [8] or using a half-cavity [5] was realised. Time-resolved measurements exhibit XRL pulses of 100 ps for the Ne-like Zn, however, without analysing the stability over numerous consecutive shots [5]. This contribution demonstrates that a half-cavity Zn XRL, pumped by a 600 J/450 ps laser, has an excellent stability in the beam quality in a series of 110 shots thus representing a robust tool suitable for applications. It is shown that one multi-layer mirror is sufficient for>100 shots without re-aligning the half-cavity. The beam stability of a double-pass XRL is investigated under the condition that the prepulse and the half-cavity geometry are fixed. The remaining shot-to-shot fluctuations of the beam divergence, symmetry, and pointing angle are analysed. The obtained results are discussed using χ^2-tests, assuming Gaussian distributions.

2 Experimental arrangement

The experiments were performed at PALS [17,18], where the asterix iodine laser, originally developed [19] at the Max-Planck-Institut für Quantenoptik (Garching) was installed. The asterix was used in Garching for XRL research already several years ago [3,20,21]. This laser delivers 600 J in 0.5 ns in the infrared at 1315 nm. The experimental arrangement including the mainly used components is shown in [22]. Two different focusing optics produce a narrow line focus. The main beam is focussed by an asphere combined with a cylindrical lens matrix consisting of 10 cylindrical lenses assembled as two arrays of five lenses (5×2 matrix). The line focus is 3 cm long and ∼130 μm wide. The prepulse guided separately to the target chamber is focussed by a second optics consisting of a spherical and a cylindrical lens. The independent focussing has the unique advantage that both line foci can be modulated separately. The 35-mm long prepulse line was slightly defocused to a width of $\sim 700\,\mu$m, so that the centre of the pre-plasma is rather uniform. The width, uniformity and superposition of both line foci was controlled by an off-axis X-ray pinhole CCD camera imaging the incoherent X-rays emitted from the plasma. An electronic device using two fast InGaAs photo-diodes controls the pepulse delay at every shot. The response time-gap between both diodes was measured on a 3-GHz Tektronix scope. This prepulse monitor is able to detect parasitic prepulses of the pump laser at a contrast of 10^{-4}, however, in fact parasites didn't appear during our experiments. Flat 3-cm wide polished Zn targets were used. The half-cavity mirror was a flat Mo/Si multi-layer having a layer period of 11.1 nm and a diameter of 25 mm. At 21.2 nm a reflectivity of 30% was measured [18]. The distance between multi-layer mirror and target edge was 8.5 mm. The unused mirror surface was protected by a 1-mm thick shield having a pinhole as a gap for the XRL beam. Since after each shot the mirror surface was damaged in a 1-mm spot the mirror was moved behind the shield without changing the half-cavity geometry. This procedure enables 100 shots with a single mirror [22].

The diagnostics was a spectrometer and a footprint detector. The beam was switched between both by the means of a flat retractable Mo/Si multi-layer mirror having a layer period of 16.7 nm and working at 45°. The spectrometer was a Wadsworth type consisting of a curved grating (900 l/mm) and a phosphor coupled to a cooled CCD [18]. To avoid detector saturation at half-cavity shots we used a 1.5-μm Al filter. A second diagnostics detected a far-field pattern (footprint) of the XRL beam. A Mo/Si multi-layer mirror reflects the X-ray beam onto a 38-mm diameter phosphor. The path length from the target to the phosphor *via* the mirror is 1.1 m. The phosphor (grain-size $< 3\ \mu$m) was a Gd_2O_2S:Tb aluminised with a 50-nm thick layer, hence insensitive in the visible. The phosphor is protected against scattered light by a metal tube thus only the radiation reflected by the multi-layer mirror is illuminating the phosphor. A CCD working in the visible records the footprint. A hair-cross of 120-μm-wires served as a fiducial. The experiment had the following order. The prepulse was optimised for single pass using the spectrometer. Then the half-cavity was optimised. Finally the beam quality was studied using the footprint diagnostics. At any shot the pump energy was measured. Additionally at some shots a Hamamatsu C7700 streak camera equipped with a S-1 photo-cathode and thus working in the infrared recorded the pump pulse duration.

In a first application experiment we demonstrated the usefulness of the double-pass amplified Zn XRL in a wavefront-splitting interferometer constructed by the Laboratoire de spectroscopie atomique et ionique, Université Paris-Sud, Orsay, France [23]. The main parts of the interferometer are a Fresnel double-mirror, consisting of two plane, polished silica mirrors, and a CCD detector. The angle between the two mirrors is 5.4 mrad. The both mirrors reflect the X-ray beam at a grazing angle of 6 degrees. To resolve the fringes the CCD was exposed under grazing incidence [18].

3 Experimental results

3.1 A brief overview of the two-weeks experimental campaign

During the two weeks we carried through altogether 145 shots with the asterix pump laser at which we observed the Zn XRL activity at 21.2 nm. At 110 shots we installed the half-cavity and at 35 shots we observed single-pass amplification.

As an overview, the distribution of the pump energies for the 145 XRL shots is plotted in a histogram showing an asymmetric distribution (Fig. 1). It is remarkable, that lasing was observed still at rather small pump energy of 284 J with a pump power of only 0.6 TW.

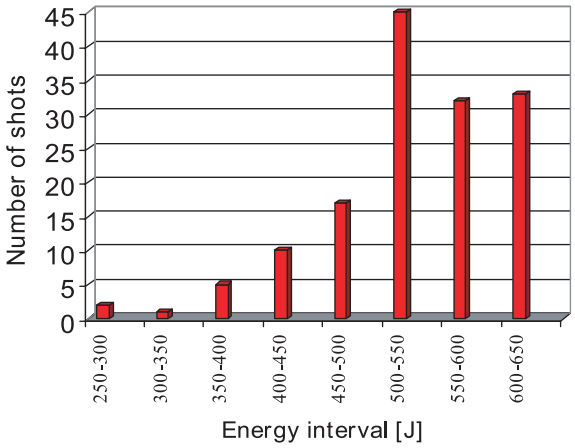

Fig. 1. Histogram of the input pump laser energy for 145 shots inducing lasing at 21.2 nm.

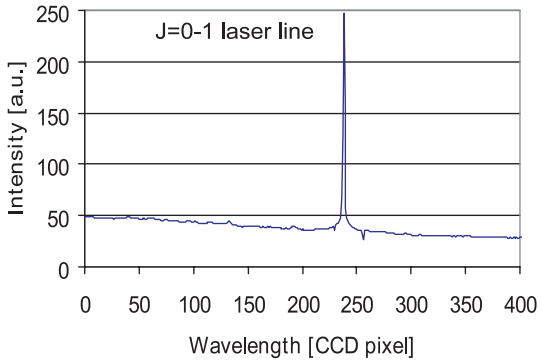

Fig. 2. The neon-like Zn laser line at 21.2 nm is completely dominating the spectrum.

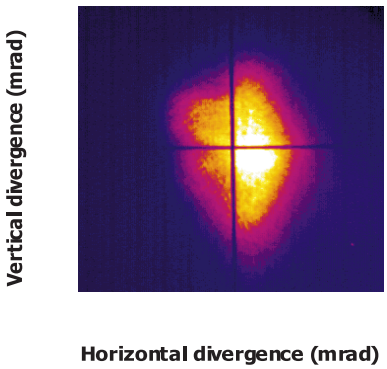

Fig. 3. Far-field pattern (footprint) of the double-pass amplified 21.2-nm XRL beam produced in the half-cavity. The target surface is on the left hand. The crossed shadows are due to the fiducial wires.

We executed three different types of measurements (as mentioned in Sect. 2). The three detectors used are giving complementary informations. The Wadsworth spectrometer gives the time-integrated line intensity and by integrating along the angular direction a relative estimate of the output energy. The far-field detector (to be called the footprint monitor) gives information of the beam profile in two dimensions, as well as the divergences in horizontal and vertical direction, the beam symmetry and the pointing angle with respect to the target surface. For the pointing angle we take the point of maximum intensity of the beam, which need not to be automatically in every case exactly the "centre" of the beam.

A typical spectrum obtained at single-pass amplification is shown in Figure 2. The laser at 21.2 nm clearly dominates the spectrum, thus the negligible background enabled us to record footprints. The footprint data do not allow energy measurements because we don't know the efficiency of our detector and therefore we cannot make an absolute calibration.

Using the Fresnel double-mirror interferometer [23] we see the fringe patterns induced by the coherent XRL beam, but, unfortunately, we block our other beam detectors in this application. The fringe visibility can be used to extract the spatial coherence of the beam, which is discussed elsewhere [18]. On the other hand the origin of the remaining scattering in the observed fringe contrast from shot-to-shot is not clear [18].

Summarising, from the 110 half-cavity shots we analysed 48 at the Wadsworth spectrometer, 20 at the footprint monitor, and 42 were used at the Fresnel interferometer.

3.2 Results of a one-day experiment applying a fixed set-up

For the statistical analysis we take the 18 XRL shots achieved and monitored with the footprint detector during one single day. Having a fixed set-up for the half-cavity multi-layer mirror and the target mounting and stable prepulse features (*level, delay and focusing*), there is the best confidence into the data. An opening of the vacuum chamber was not necessary during the whole day.

The results were obtained using a 1.6 J prepulse, followed after 10 ns by the main pulse at an irradiance of $\sim 2.8 \times 10^{13}$ Wcm^{-2}. Due to the $\sim 700\,\mu$m-wide prepulse focus the pre-irradiance was $\sim 1.6 \times 10^{10}$ Wcm^{-2} which corresponds to a prepulse ratio of $\sim 6 \times 10^{-4}$. Former results confirm that this weak prepulse optimises the Zn XRL [6]. Activating the half-cavity mirror, the XRL output was attaining the mJ-regime. It is remarkable, that the half-cavity is working efficiently for pump pulses being at least 380 ps long [18]. For shorter pulses it is not guaranteed, that the inversion is lasting long enough for a whole round trip. For that reason the half-cavity length was put to the shortest feasible of 38.5 mm [20].

Figure 3 displays a typical footprint of the half-cavity Zn XRL beam. The shadows in the footprint are due to the fiducial wires. The pointing angle is 5.5 mrad and the horizontal and vertical beam divergence are 3.8 and 5.8 mrad, respectively, and thus the beam symmetry is for this footprint 0.65. The statistics carried out here in the following analyses the 18 shots of comparable half-cavity geometry. The horizontal divergence plotted in Figure 4 as a function of the pump energy exhibits small fluctuations

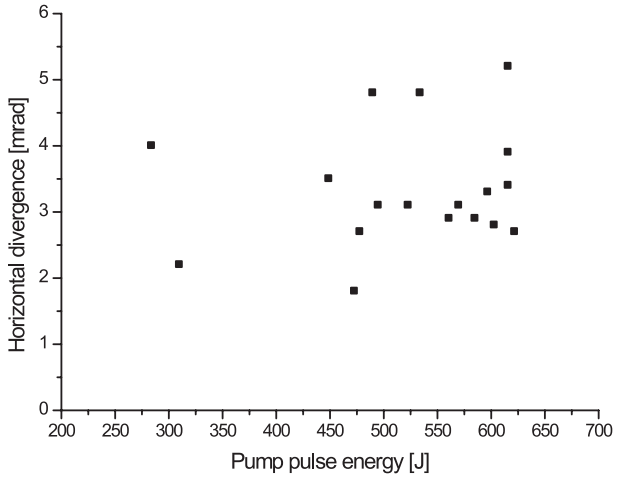

Fig. 4. Horizontal divergence of the XRL beam in units of mrad as a function of the pump laser energy.

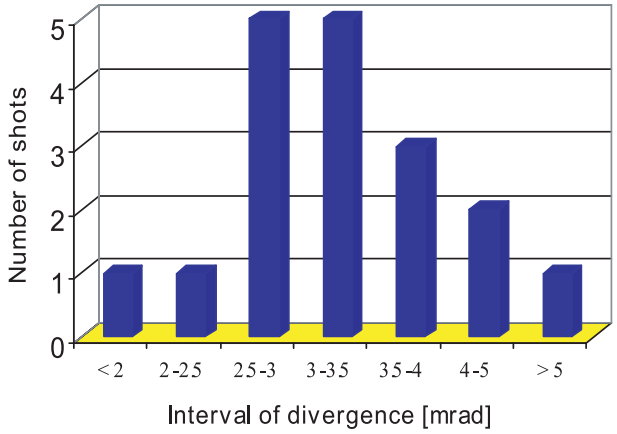

Fig. 5. Histogram representing the distribution of the beam divergence in horizontal direction according to the same shots shown in Figure 4.

mainly between 2.5 and 5 mrad. We cannot see a strong correlation with the pump energy, just the opposite, it looks random-like. Figure 5 shows the distribution of the horizontal beam divergence observed at these 18 subsequent shots. The vertical divergence can be found in [22]. The ratio of horizontal to vertical divergence qualifies the beam symmetry of which the measured values as a function of the pump pulse energy is given in Figure 6. This figure does not provide a correlation, more or less it looks random-like, this is, off course the consequence of the random-distributed divergences. Defining seven intervals we find the distribution of observed beam symmetries as plotted in Figure 7. For comparison the distribution of the measured pump laser energies for the same 18 shots is depicted in Figure 8. It shows an asymmetric distribution. The obvious and remarkable difference of both distributions is analysed by the means of a χ^2-test and discussed in the following sections.

To verify that the half-cavity is working well in the sense that amplification in the whole double-pass is achieved shots having different pump pulse durations were

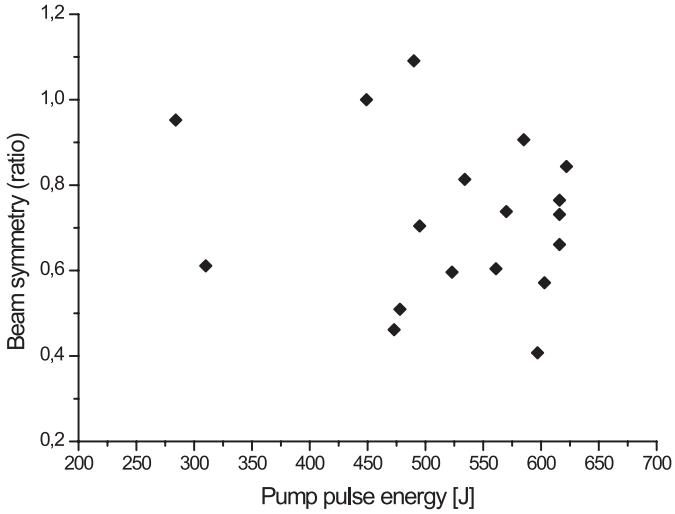

Fig. 6. XRL beam symmetry as a function of the pump pulse energy. Obviously the data points are random-like distributed and not correlated.

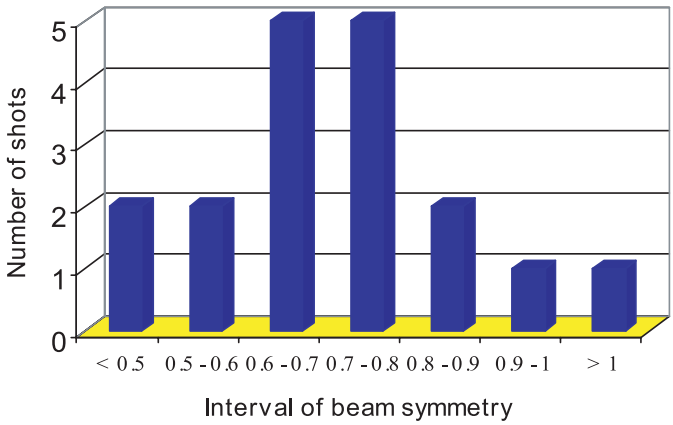

Fig. 7. Histogram illustrating the distribution of the XRL beam symmetry defined as the ratio between horizontal and vertical divergence.

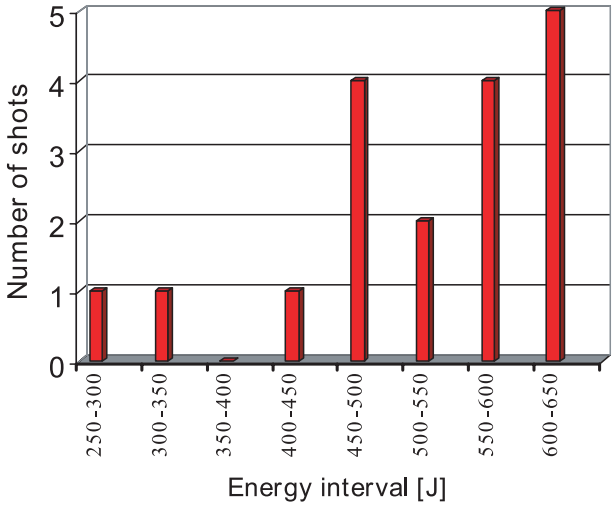

Fig. 8. Histogram showing the distribution of pump laser energy for the same shots as in Figures 4–7.

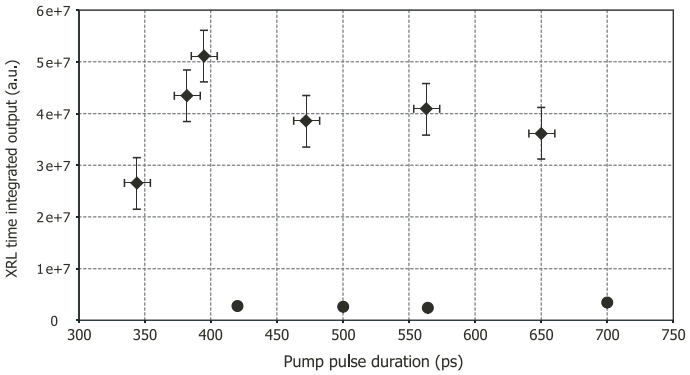

Fig. 9. Dependence of the double-pass amplified (⧫) XRL output on the pump pulse duration. The data show that pulses lasting longer than 380 ps produce sufficient gain lifetime to support a second amplification on the return path in the half-cavity. At too short pulses the efficiency of the half-cavity breaks down. For comparison single-pass data (•) are added.

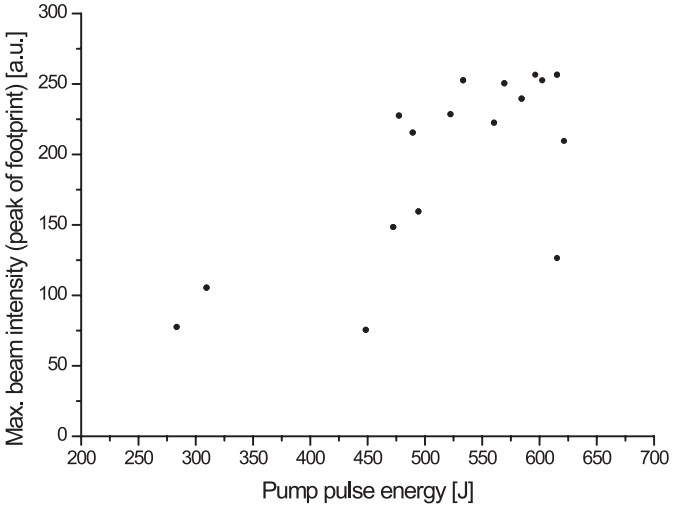

Fig. 10. Beam peak intensity as a function of pump energy. Obviously, a larger input energy leads to a larger XRL output.

analysed. It is emphasised that the round trip time of 257 ps in the half cavity is not negligible short. In Figure 9 the at the spectrometer observed dependence is displayed exhibiting a quite stable output at pulses between 400 ps and 650 ps. Below 380 ps the output decreases indicating that at such short pulses the gain lifetime is not long enough to sustain the return amplification. Thus the full efficiency of the half-cavity was observed to be maintained only at pulses longer than 380 ps. For comparison single-pass data representing a significantly lower output level are added into Figure 9.

From the data received at the far-field detector we can extract Figure 10 in which the maximum beam intensity is depicted as a function of the pump laser energy. It is evident that the maximum beam intensity increases — *despite a few exceptional points* — with the pump energy. A possible explanation for the exceptional points may be a different pump pulse shape, as observed with the Hamamatsu streak camera.

4 Statistical analysis of the XRL beam quality

The double-pass XRL output was observed to be robust and reproducible in numerous shots. We execute a statistical analysis including a χ^2-test that is used as a common tool to control the quality and reliability of products or processes. The procedure of a χ^2-test is applied onto the XRL beam quality [22]. At the beginning stands a hypothesis of the underlying distribution, in fact, we assume a Gaussian distribution. This assumption makes sense in all experiments where the errors are *randomly* distributed and independent of controllable parameters. The observed fluctuations are considered to have statistical reasons. Possible systematical errors (target quality, alignment, temperature fluctuation et cetera) are not investigated here. The χ^2-test is performed in three steps: (a) we define seven intervals and assign the experimental results to these intervals. The number of intervals leads to the degrees of freedom f of the test. (b) By assuming a Gaussian distribution we calculate the χ^2 using the formula (1). (c) We compare the result of χ^2 with a probability of making no error by accepting or rejecting the hypothesis. This probability is calculated by using equation (2). It is emphasised that the test is not telling whether the hypothesis is true or not, it is only giving a probability to accept or to reject the hypothesis. In the case of rejecting the hypothesis the test is not explaining the reasons for doing that. In the case of acceptance the test is delivering a probability for the chance of making an error, anyway. The χ^2 measures the deviation between the observed (Figs. 1, 5, 7) and the expected distribution

$$\chi^2 = \sum_{i=1}^{k} \left(\frac{(m_i - Np_i)^2}{Np_i} \right) \tag{1}$$

where k is the number of intervals, m_i is the observed number of shots (*frequency*) in the interval i, p_i is the expected probability of the interval i, and N is the total number of all shots.

The result of a statistical analysis determining the average a of all measured values, and the standard deviation s is given in Table 1 for horizontal and vertical divergence and beam symmetry. We use a and s as input parameters for a normalised Gaussian distribution. Hence, the probability p_i to find a result in the interval i is fixed through the expected distribution. The expected frequency at the interval i is Np_i. The division of the spectrum into intervals is so far free if there is no overlap and additionally the full observable spectrum is covered. Organising seven intervals (Figs. 5 and 7), and counting the frequency in each interval, we receive the f of the χ^2-test defined as $f = k - 1$ — (number of estimated parameters). Hence with $k = 7$ intervals and two parameters a and s we get $f = 4$. The χ^2-distribution described by a fundamental density function $d(y, f)$ can be found in [22]. Integration of the density function $d(y, f)$ leads to a probability $\beta(\chi^2, f)$

Table 1. Statistical parameters and results of chi-squared tests for the Zn XRL beam properties.

	horizontal divergence	vertical divergence	beam symmetry
number of shots	18	18	18
average a	3.43 mrad	4.77 mrad	0.75
standard deviation s	0.92 mrad	1.31 mrad	0.25
sum of χ^2	3.03	2.03	1.40
probability $\alpha = 1 - \beta$	0.55	0.73	0.84

for rejection of the hypothesis given in equation (2):

$$\beta(\chi^2, f) = \left(\frac{1}{2^{f/2}\Gamma(f/2)}\right) \int_0^{\chi^2} \left(\exp(-y/2) y^{\frac{f}{2}-1}\right) \mathrm{d}y = \int_0^{\chi^2} d(y, f)\mathrm{d}y \quad (2)$$

with the upper integration limit χ^2 given in equation (1). The substitution $y{:=}\ \chi^2$ is used for simplification and Γ denotes the gamma-function. At fixed f with higher χ^2 the rejection probability β is enlarged. For $f = 4$ the integration can be solved analytically and we receive

$$\beta = 1 - (2 + y)\exp(-y/2)/2. \quad (3)$$

The acceptance probability α of the hypothesis is $\alpha = 1 - \beta$. With extended χ^2 the α will be smaller. The density function $d(\chi^2, 4)$ and the probability function $\beta(\chi^2, 4)$ are plotted in [22] for $f = 4$. If χ^2 is above threshold the hypothesis should be rejected. Conversely the hypothesis can be accepted. Customarily there is set a critical probability level above that the hypothesis will be rejected, *e.g.*, $\beta = 0.50$ or $\beta = 0.95$. In the latter case remains a 5%-error when the hypothesis is rejected. For $f = 4$ the thresholds are $\chi^2 = 3.36$ ($\beta = 0.50$) and $\chi^2 = 9.49$ ($\beta = 0.95$), respectively. Particularly, if the sample is small (<100) or the frequency in some intervals is <3, this can lead to an over-estimation of χ^2 and thus to an under-estimation of the acceptance probability. Thus we will not accept the hypothesis careless. Clearly the statistics will be improved with increasing number of shots. The execution of the χ^2-test is given in detail in [22] for the beam symmetry and the observed divergences of the half-cavity Zn XRL. The result for the beam symmetry is $\chi^2 = 1.4$. Using (3) we calculate $\beta = 0.16$ and $\alpha = 0.84$. For the divergences the corresponding results are listed in Table 1.

Concerning the beam symmetry, the horizontal and the vertical divergences β is less than the critical level: the hypothesis can be accepted, because there is no significance for rejection. In the case of rejection we have a probability error of more than 55% for these beam parameters as given in Table 1. This is the only argument to accept the hypothesis. It is not clear, whether the hypothesis is really true. But from the statistical point of view the Gaussian distribution seems to be authentic. In the opposite if β would be higher than the critical level the hypothesis would be rejected doing an error of $< \alpha$%. This case is not fulfilled here. Considering the both beam divergences and the beam symmetry there is no argument to reject the hypothesis. An objection that the χ^2-test is favouring the acceptance of hypothesis can be enfeebled when the pump energy showing an asymmetric-shaped distribution is analysed (Fig. 1). Here the statistics is improved using the larger random sample of all 145 laser shots. A mean energy of 523 J and a standard deviation of 97 J are extracted. A χ^2-test gives $\chi^2 = 22.5$, $\beta = 0.999$ and hence $\alpha < 0.1$%. The Gaussian-hypothesis must be rejected obviously. The pump energy is definitely not random-distributed. That means that the XRL demonstrates a higher stability than the drive laser, confirming additionally that the double-pass Zn XRL is saturated [18].

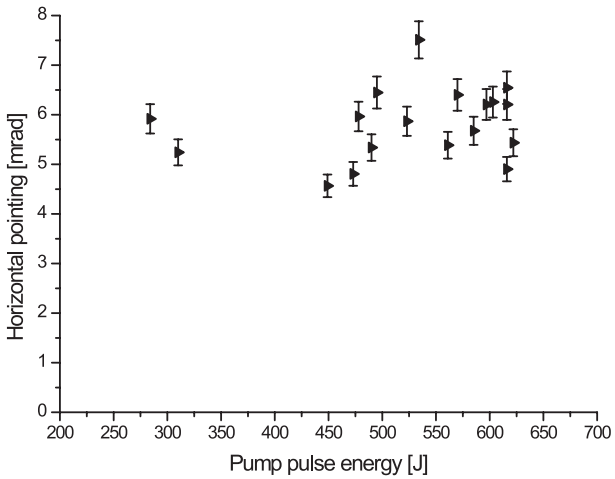

Fig. 11. XRL beam pointing angle with respect to the target surface as observed at different pump pulse energies. The data are concentrated between 4.5 and 6.5 mrad.

However, the pointing angle of the XRL beam is *within the measurement accuracy* almost comparable for all the half-cavity shots having a value around (5.5±1) mrad in relation to the target surface. This is illustrated in Figure 11. Notifying the accuracy of our measurement (error bars) we can define only intervals having at least the width of 0.5 mrad. The corresponding histogram is shown in Figure 12. The four intervals between 4.5 and 6.5 mrad exhibit almost the same frequency. It seems that these intervals contribute with the same probability and thus for this almost rectangular-distributed pointing a chi-squared test assuming a Gaussian distribution makes no sense. Indeed, the pointing angle is only quite stable for re-injection angles between 1 and 5 mrad [18]. It is surprising that these rather small re-injection angles enable the half-cavity to compensate the XRL beam refraction after the first pass in the expanding plasma. By way of contrast, a wide scattering of deflection angles was observed in [16] for the TCE nickel-like Ag laser evaluating

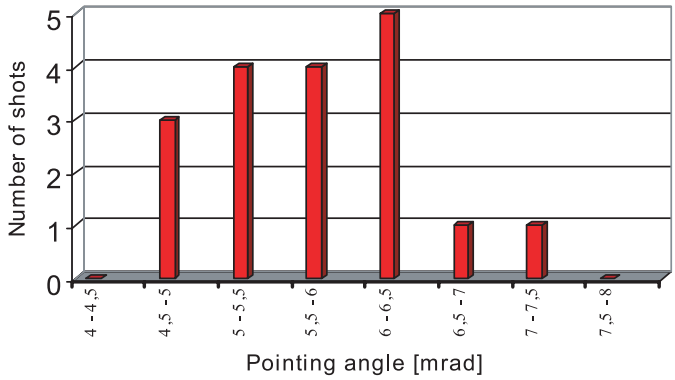

Fig. 12. Histogram of the pointing angle observed at the 18 half-cavity shots (see Figs. 4–8). The four intervals between 4.5 and 6.5 mrad exhibit almost the same frequency (nearly rectangular-distribution).

altogether 15 (single-pass) shots under traveling-wave irradiation. Thus the in this work observed stability seems to be related to the high-gain region in the plasma due to the saturation in the specific half-cavity configuration. Using a angular-resolved scan of the mirror tilt, as discussed in [18] it can be extracted that the gain region has a size of approximately 50 μm. To clarify the details of the gain-profile it is planned to improve the diagnostics by installing a near-field imaging system.

5 Outlook

To characterise the full beam profile in two dimensions there is a possibility by evaluating the so-called Times Diffraction Limit M^2-factor as used frequently to describe the beam quality of semiconductor lasers [24] emitting in the visible or in the infrared. For the XRL this can be an object of further investigations. On the other hand the presented double-passed Zn XRL is surely not a single-mode laser.

External research groups who want to make application experiments using the 21.2-nm Zn XRL can apply for beamtime at PALS (`www.pals.cas.cz`). Using other target materials and the corresponding multilayer mirrors also other wavelengths will be available.

6 Summary and conclusion

The beam quality of a half-cavity Zn XRL (21.2 nm) delivering stable output over many shots is studied in a statistical analysis including χ^2-tests. At fixed half-cavity geometry the hypothesis that the divergence is Gaussian distributed is confirmed. The 450-ps long pump pulse was adequate to maintain the inversion over the whole roundtrip in the 38.5-mm short half-cavity usable routinely without exchange of any component. Protecting the unused mirror surface we performed 110 consecutive shots. High reproducibility recommends this XRL as a robust tool for applications. The Zn XRL had a nearly symmetrical beam at a stable pointing angle. This enables applications applying 3 reproducible shots per hour. It is planned to allocate XRL beam time to external scientists. Concluding, the narrow-scattered XRL beam quality compared with the rather wide-scattered input pump energy illustrates an impressive stability of the saturated half-cavity Zn XRL having an output energy of max. 4 mJ.

Fundamental and technical support of J. Moravec, J. Sobota, M. Pfeifer, J. Ullschmied, and K. Jungwirth is greatly appreciated. We thank G. Jamelot, J.C. Lagron, D. Ros, D. Joyeux, and D. Phalippou for the cooperation at the PALS user project no. 17. This work was financed from the EU Access to Research Infrastructures Grant HPRI-00108, from the Research Centres Project LN00A100, and from the Academy of Sciences of the Czech Republic Grant A1010014.

References

1. J.J. Rocca, J. Dunn, S. Suckewer, *8th Int. Conf. on X-Ray Lasers*, AIP Conf. Proc., p. 641 (2002)
2. J. Nilsen, B.J. MacGowan, L.B. DaSilva, J.C. Moreno, Phys. Rev. A **48**, 4682 (1993)
3. Y. Li, G. Pretzler, E.E. Fill, Phys. Rev. A **51**, R4341 (1995)
4. A.R. Präg, F. Löwenthal, J.E. Balmer, Phys. Rev. A **54**, 4585 (1996)
5. B. Rus *et al.*, Phys. Rev. A **55**, 3858 (1997)
6. A.R. Präg, F. Löwenthal, R. Tommasini, J.E. Balmer, Appl. Phys. B **66**, 561 (1998)
7. J. Zhang *et al.*, Science **276**, 1097 (1997)
8. S. Sebban *et al.*, Phys. Rev. A **61**, 043810 (2000)
9. P.V. Nickles *et al.*, Phys. Rev. Lett. **78**, 2748 (1997)
10. J. Dunn, Y. Li, A.L. Osterheld, J. Nilsen, J.R. Hunter, V.N. Shlyaptsev, Phys. Rev. Lett. **84**, 4834 (2000)
11. R.E. King *et al.*, Phys. Rev. A **64**, 053810 (2001)
12. A. Klisnick *et al.*, Phys. Rev. A **65**, 033810 (2002)
13. J.J. Rocca, D.P. Clark, J.L.A. Chilla, V.N. Shlyaptsev, Phys. Rev. Lett. **77**, 1476 (1996)
14. J.J. Rocca, Rev. Sci. Instr. **70**, 3799 (1999)
15. B.E. Lemoff, G.Y. Yin, C.L. Gordon, C.P.J. Barty, S.E. Harris, Phys. Rev. Lett. **74**, 1574 (1995)
16. J. Kuba *et al.*, Phys. Rev. A **62**, 043808 (2000)
17. K. Jungwirth *et al.*, Phys. Plasmas **8**, 2495 (2001)
18. B. Rus *et al.*, Phys. Rev. A **66**, 063806 (2002)
19. H. Baumhacker *et al.*, Appl. Phys. B **61**, 325 (1995)
20. A.R. Präg, A. Glinz, J.E. Balmer, Y. Li, E.E. Fill, Appl. Phys. B **63**, 113 (1996)
21. Y. Li, G. Pretzler, P.X. Lu, E.E. Fill, J. Nilsen, Phys. Plasmas **4**, 479 (1997)
22. A.R. Präg, T. Mocek, M. Kozlová, B. Rus, G. Jamelot, D. Ros, Eur. Phys. J. D **22**, 31 (2003)
23. J. Svatos, D. Joyeux, D. Phalippou, F. Polack, Opt. Lett. **18**, 1367 (1993)
24. A.E. Siegman, *Lasers* (University Science Books, Mill Valley, CA, 1986)